Journal of Zhejiang University-SCIENCE B (Biomedicine & Biotechnology) in press
www.jzus.zju.edu.cn; www.springer.com/journal/11585
E-mail: jzus_b@zju.edu.cn

Research Article

https://doi.org/10.1631/jzus.B2500216

Reduced NGF mediates arsenic-induced mitochondrial dynamic imbalance and neuronal damage both in vivo and in vitro

Xinbo MA[1,2,3,4], Liu YANG[1,3,4], Xinhua SHAO[1,3,4], Jia CUI[1,3,4], Ziqiao GUAN[1,3,4], Man LV[1,3,4], Shuaifei YANG[1,3,4], Na FANG[1,3,4], Yang LIU[1,3,4], Yanhui GAO[1,3,4], Xiaona LIU[1,3,4]✉, Yanmei YANG[1,3,4]✉

[1]*Center for Endemic Disease Control, Chinese Center for Disease Control and Prevention, Harbin Medical University, Harbin 150081, China*
[2]*Xi'an Center for Disease Control and Prevention, Xi'an 710000, China*
[3]*NHC Key Laboratory of Etiology and Epidemiology (Harbin Medical University), Harbin 150081, China*
[4]*Joint Key Laboratory of Endemic Diseases (Harbin Medical University, Guizhou Medical University, Xi'an Jiaotong University), Harbin 150081, China*

Abstract: Arsenic exposure is known to cause cognitive deficits, although the underlying mechanisms are yet to be explored. In this study, we investigated the role of nerve growth factor (NGF), a neuroprotective factor, in arsenic-induced cognitive impairment. In mouse models exposed to 25 mg/L and 50 mg/L sodium arsenite ($NaAsO_2$), we observed neuronal damage accompanied by the downregulation of NGF, decreased phosphorylation of phosphatidylinositol 3-kinase/protein kinase B (PI3K/AKT), reduced phosphorylation of the mitochondrial fission protein dynamin-related protein 1 (Drp1), and downregulation of the mitochondrial fusion protein optic atrophy 1 (OPA1). Similarly, the downregulation of NGF, inactivation of the PI3K/AKT signaling pathway, mitochondrial dynamics imbalance (dysregulation of mitochondrial fission and fusion processes), and increased apoptosis were observed in HT-22 cells exposed to 4 μmol/L $NaAsO_2$. NGF overexpression mitigated these arsenic-induced alterations, while the protective effect of NGF against arsenic toxicity was reduced by LY294002, a PI3K/AKT pathway inhibitor. These findings suggest that a decrease in NGF mediates the arsenic-disrupted mitochondrial dynamics via inhibiting the PI3K/AKT pathway, ultimately impairing cognitive function.

Key words: Arsenic; Nerve growth factor (NGF); Mitochondrial dynamics; Neurotoxicity; Phosphatidylinositol 3-kinase/protein kinase B (PI3K/AKT)

1 Introduction

Arsenic, a naturally occurring toxic metalloid, primarily enters the human body through contaminated water, food, soil, and atmospheric deposition (Sevak and Pushkar, 2024; Xing et al., 2024). Globally, more than 200 million people consume drinking water with arsenic levels exceeding 10 μg/L—the maximum limit set by the World Health Organization (WHO) —making arsenic exposure a significant public health concern (Bozack et al., 2019; Peel et al., 2022). Epidemiological studies have reported significant reductions in verbal IQ, spatial memory and long-term memory in children chronically exposed to arsenic concentrations above 10 μg/L in drinking water (Hong et al., 2014; Liu and Bain, 2018). A cross-sectional research including 1,556 adults in China also identified a negative correlation between hair arsenic levels and Mini-Mental State Examination (MMSE) scores, suggesting that arsenic may be an independent risk factor for cognitive impairment (Wang et al., 2021). Moreover, exposure to drinking water containing 100 μg/L arsenic for 2 weeks severely impaired the

✉ Xiaona LIU, xiaonaliu_2013@163.com; Yanmei YANG, yangyanmei@hrbmu.edu.cn
Xiaona LIU, https://orcid.org/0000-0002-9856-0801
Yanmei YANG, https://orcid.org/0000-0001-9531-4253

Received Apr. 28, 2025; Revision accepted Aug. 11, 2025;
Crosschecked xxx. xx, 20xx; Published online xxx. xx, 20xx

spatial and contextual memory of mice (Cronican et al., 2013). These observations indicate that prolonged arsenic exposure is positively associated with cognitive impairment; however, the specific mechanisms underlying this damage remain unclear.

Arsenic has been reported to exert toxic effects on brain mitochondria (Prakash et al., 2016). Mitochondria are highly dynamic organelles that undergo continuous fission and fusion processes, collectively known as mitochondrial dynamics, to maintain normal function (Fei et al., 2019; Mu et al., 2019). The balance of mitochondrial dynamics is crucial for neuronal development, plasticity and function, while an imbalance thereof can lead to mitochondrial dysfunction, disrupted neuronal activity, cognitive impairment, and other neurodegenerative conditions (Bertholet et al., 2016; Chen et al., 2023). The regulation of mitochondrial dynamics involves multiple regulatory proteins, including dynamin-related protein 1 (Drp1) and mitochondrial fission protein 1 (Fis1), which mediate mitochondrial fission, as well as optic atrophy 1 (OPA1) and mitochondrial fusion proteins 1 and 2 (Mfn1/2), which mediate mitochondrial fusion (Yapa et al., 2021). A decrease in Drp1 reduced the number of forebrain synapses and impaired the development of primary neuronal cells in mice, while a deficiency in OPA1 induced neuronal apoptosis and mitochondrial dysfunction (Lai et al., 2020). Drp1 phosphorylation at Ser616 plays an important role in regulating mitochondrial fission and neurodevelopment, and the phosphorylation status of Ser616 directly affects mitochondrial dynamic balance (Gao et al., 2022a). Research indicates that arsenic can impair mitochondrial function by causing excessive mitochondrial fission in myocardial cells, leading to irreversible damage to myocardial differentiation and embryonic development (Jeong et al., 2023). In addition, arsenic toxicity in testes and germ cells has been linked to the disruption of mitochondrial fusion and fission (Ye et al., 2023). Related research has shown that arsenic exposure leads to a significant decrease in the phosphorylation levels of phosphatidylinositol 3-kinase (PI3K), protein kinase B (AKT) and its downstream mammalian target of rapamycin (mTOR), thereby relieving the inhibition of autophagy, eventually inducing ferroptosis and autophagic cell death, and that this pathway inhibition will also disrupt mitochondrial dynamic balance (Liu et al., 2020; Lu et al., 2023b; Lu et al., 2024). However, the precise mechanisms by which arsenic disrupts mitochondrial dynamics remain unclear, particularly regarding the key regulatory proteins involved in this process.

Nerve growth factor (NGF), the first identified neuroprotective regulator within the neurotrophic factor family (Baruch-Eliyahu et al., 2019), plays a crucial role in neurogenesis and nerve regeneration by regulating mitochondrial dynamics, reorganizing mitochondrial networks, and maintaining mitochondrial mass, membrane potential and bioenergetic capacity (Martorana et al., 2018). Specifically, NGF enhances mitochondrial fusion and fission by increasing phosphorylated dynamin-related protein 1 (p-Drp1) and OPA1 levels, leading to alterations in the mitochondrial length and density, thereby maintaining neurons in a highly active state to accommodate the energy requirements of normal neuronal growth (Martorana, et al., 2018). NGF exerts dual biological functions—promoting neuronal trophism and adaptive growth—and plays a critical regulatory role in the survival, development, function, and plasticity of central neurons (Sung et al., 2018; Cho et al., 2020). NGF binds to its receptor tyrosine kinase A (TrkA) and exerts neuroprotective effects by activating downstream signaling molecules such as phosphorylated PI3K/AKT(Marlin and Li, 2015; Yan et al., 2020). Numerous studies have demonstrated that the NGF/TrkA signaling pathway is essential for the plasticity and survival of forebrain cholinergic neurons in the hippocampus and cortex (Sanchez-Infantes et al., 2018), regions responsible for learning and memory. The upregulation of NGF/TrkA has been shown to mitigate radiation-induced neurogenesis deficits and cognitive impairments by activating PI3K/AKT signaling (Ji et al., 2020). In populations with cognitive impairments, including individuals with intellectual disabilities, serum NGF levels have been found to be significantly lower than in healthy individuals. Consequently, NGF has been recognized as a potential serum biomarker for intellectual disability (Tuon et al., 2023; Malewska-Kasprzak et al., 2024). It has been reported that exogenous NGF supplementation can effectively prevent arsenic-induced neurotoxicity in PC12 cells by activating AKT-related pathways (Tan et al., 2019). However, whether arsenic affects NGF levels in humans and whether NGF downregulation contributes to arsenic-induced mitochondrial dynamics imbalance remain to be elucidated.

In this study, we investigated whether arsenic exposure leads to a decrease in NGF, thereby inducing mitochondrial dysregulation, neuronal damage and cognitive impairment. Furthermore, using both a mouse model and HT-22 cells, we examined whether inactivation of the PI3K/AKT signaling pathway mediates these detrimental effects. Finally, through cell-based experiments, we explored the mechanistic role of this pathway in arsenic-induced neurotoxicity. Our findings provide a theoretical foundation for understanding the mechanisms of arsenic-induced neurotoxicity and may inform future therapeutic strategies.

2 Materials and methods

2.1 Reagents

Sodium arsenite ($NaAsO_2$) was purchased from Sigma-Aldrich (Saint Louis, USA). Detailed information regarding other reagents is provided in Table S1.

2.2 Cell culture and animal experimental procedures

2.2.1 Cell culture and transfection

HT-22 cells (Procell, Wuhan, China) were seeded at a density of 2×10^5 cells per 25 mL culture flask and incubated for 12 h. A mixture was prepared containing 400 μL of NGF lentivirus (GenePharma, Shanghai, China) stock solution with a concentration of 1×10^9 TU/mL and 3600 μL of DMEM medium containing 10 g/L FBS, to form a final concentration of 1×10^8 TU/mL. After thorough mixing, 3.6 mL of 1640 (GIBCO, Invitrogen, Carlsbad, USA) supplemented with 10% FBS and 5 μg/mL polyamine was added. Following incubation at 37℃ and 5% CO_2, cell status was assessed. Successfully transfected cells were selected using 1 μg/mL puromycin (Solarbio, Beijing, China) for an additional 24 h. The experiments revealed that treatment with 2 μmol/L $NaAsO_2$ significantly induced apoptosis in HT-22 cells, while exposure to 4 μmol/L $NaAsO_2$ reduced the cell survival rate to below 50%. Therefore, we chose these two concentrations for our study.

2.2.2 Cell counting kit-8 (CCK-8) assays

Cell viability was measured using the CCK-8 Assay Kit (Biosharp, Hefei, China). HT-22 cells were cultured at a density of 3000 cells/well in a 96-well plate and incubated at 37℃ with 5% CO_2 for 24 h. Once cell adhesion was complete, cells were exposed to varying concentrations of arsenic for 24 h. Absorbance at 450 nm was measured using a microplate reader (Bio-Rad, California, USA) following the manufacturer's protocol.

2.2.3 Cell apoptosis assay

Cell apoptosis was detected using the Annexin V-FITC Apoptosis Detection Kit (BD, New York, USA). 10 μL of PI, 5 μL of membrane associated Annexin V, and 500 μL of 1× binding buffer were added to each bottle of HT-22 cells (1×10^5 cells), which were then resuspended and incubated for 12 min. The fluorescence intensity of cells was analyzed using a flow cytometer (BD Accuri C6 Plus, USA). FlowJo V10 was used to calculate the number of cells in different states.

2.2.4 Western blot

Total protein was extracted using RIPA lysis buffer (Beyotime, Shanghai, China) containing protease (Roche, Indianapolis, USA) and phosphatase inhibitors (Beyotime, Shanghai, China). After lysis, the supernatant was collected by centrifugation and the protein concentration was quantified using BCA assay kit (Beyotime, Shanghai, China). Electrophoresis (80 V constant voltage) and membrane transfer (200 mA constant current) were run for durations adjusted to the molecular weights of the protein. Equal protein amounts were separated and blocked overnight. Membranes were incubated with primary and secondary antibodies, washed and developed using an ECL solution, then incubated with secondary antibodies and visualized using an enhanced chemiluminescence (ECL) detection system (Biosharp, Hefei, China). Goat anti-rabbit or anti-mouse IgG was

purchased from ZSGB-BIO (Beijing, China). Equal proportions of A and B solutions were mixed to prepare ECL color solution. The PVDF membrane (Roche, Indianapolis, USA) was soaked in a dark solution for 1 min and scanned for color development. Protein blot images were captured by the Tanon 5200 Multi-Chemiluminescence Imaging System (Tanon, China) and quantified with ImageJ 2.0 software (USA). The detailed information of the antibodies used is shown in Table S2.

2.2.5 Immunofluorescence staining

Cells were washed three times, fixed with 4% paraformaldehyde and incubated overnight at 4 ℃ with primary antibodies. Afterwards, cells were incubated with a secondary antibody for 1 h. The details and dilution concentrations of antibodies are listed in in Table S2. The observation was done using a Zeiss confocal laser scanning microscope (Carl Zeiss AG, Baden-Wuberg, Germany). Zeiss Zen software was utilized to capture images.

2.2.6 Transmission electron microscopy (TEM)

Glutaraldehyde was used to fix HT-22 cells, which were stored at room temperature away from light for 30 min and then transferred to 4℃. After staining, they were observed under a TEM (H-7650, Hitachi, Japan).

2.2.7 Design of animal experiment

The animal experimental design is shown in Fig. 1a. Forty 4-week-old male C57BL/6N mice were purchased from Charles River Experimental Animal Technology Co., Ltd. (Beijing, China), as this age marks a critical period of maturation of the nervous system. After one week of adaptive feeding, the mice were randomly divided into three groups of 10 each. The control mice were given distilled water, while the mice in the $NaAsO_2$ group were given 25 mg/L or 50 mg/L $NaAsO_2$ for 12 weeks. The dosage of arsenic was selected based on our team's previous research (Lv et al., 2023). The experimental protocol was approved by the Ethics Committee of Harbin Medical University (Ethics Number: HRBMUECDC20210902).

2.2.8 Morris water maze (MWM) test

The learning and memory abilities of mice were evaluated using the Morris water maze. The platform is located in the middle of one quadrant of the test pool. The mice were randomly placed in one quadrant, and the time and trajectory of finding the platform are recorded: if it exceeded 60 s, the mice were guided to stay on the platform for 10 s. The mice were trained 4 times a day for a total of 4 days. On the 5th day, the platform was dismantled and the 60s movement trajectory was observed. The trajectory is recorded by SMART 2.5 software (Panlab, Spain).

2.2.9 Determination of arsenic content in samples

Hydride generation-atomic fluorescence spectrometry (HG-AFS) (AFS-933, Beijing Jitian Instruments Co., Ltd.) was employed to detect the total arsenic content in urine and brain tissues of mice. Specifically, 5% hydrochloric acid solution was used as the carrier solution and 2% potassium borohydride as the reducing agent to detect the absorbance values (OD) of each sample and standard. Finally, the arsenic content of samples was obtained by the standard curve.

2.2.10 H&E staining, TUNEL staining and Nissl staining

The paraffin-embedded tissues were sectioned to 4 μm thickness, and the slices were stained with hematoxylin and eosin (H&E) (Biosharp, Hefei, China), terminal deoxynucleotidyl transferase dUTP nick-end labeling (TUNEL) detection reagents (Roche, Indianapolis, USA), and Nissl detection reagents (Solarbio, Beijing, China). The results were observed under a light microscope (Olympus BX53, Japan). The TUNEL and Nissl staining results were analyzed by Image Pro Plus 6.0 software.

2.2.11 Immunohistochemistry staining

The immunohistochemical steps were referred to the methods used in our previous studies (Ding et al., 2023). The detailed information of the antibodies used is shown in Table S2. Hippocampal tissues were observed under a microscope (Olympus BX53, Japan), and protein expression in the cells was quantified and analyzed using Image Pro Plus 6.0 software.

2.3 Statistical analysis

The Morris water maze escape latency data were analyzed using repeated-measures ANOVA. The long axis (the longest diameter) and short axis (the longest diameter perpendicular to the long axis) of each mitochondrion in the TEM field of view were measured using ImageJ software. At least three independent biological replicates were selected for each group of samples, with three TEM images taken for each replicate. The aspect ratio was calculated as the long axis length divided by the short axis length. Comparisons among multiple groups were analyzed using one-way ANOVA. $P<0.05$ was considered statistically significant.

3 Results

3.1 Effects of $NaAsO_2$ on brain-to-body ratio and cognitive performance in mice

In order to investigate the effects of arsenic exposure on body weight, brain arsenic accumulation and cognitive function in mice, mice were subjected to a 12-week $NaAsO_2$ treatment and their neurotoxic effects were evaluated through brain-to-body ratio analysis and the Morris water maze test. At the end of the 12th week, the body weights of mice treated with 25 mg/L and 50 mg/L $NaAsO_2$ were significantly lower than those in the control group ($P<0.05$ and $P<0.001$; Fig. 1b). In contrast, the brain-to-body ratios of mice treated with 50 mg/L $NaAsO_2$ were significantly higher than those in the control group ($P<0.001$; Fig. 1c). Compared to the control group, the brain total arsenic levels of mice treated with 25 mg/L and 50 mg/L $NaAsO_2$ were significantly increased ($P<0.001$; Fig. 1d). Similarly, the urine tAs level in these groups were significantly higher than those in the control group ($P<0.05$ and $P<0.001$; Fig. 1e).

In the MWM trails, the time required for mice to locate the hidden platform decreased with training progression (Fig. 1f). On the 5th day of the space exploration test (SPT), mice treated with 25 mg/L and 50 mg/L $NaAsO_2$ exhibited a significantly lower frequency of platform crossings ($P<0.01$ and $P<0.001$, Fig; 1g) and reduced time spent in the target quadrant compared to the control mice ($P<0.01$ and $P<0.001$; Fig. 1h). In addition, the movement distances of mice in the 50 mg/L $NaAsO_2$ group within the target quadrant were significantly shorter than those of the control mice ($P<0.05$; Fig. 1i). As shown in Fig. 1j, the trajectories of the control mice are concentrated around the platform location, whereas those of $NaAsO_2$-treated mice are more dispersed. These results indicate that increasing $NaAsO_2$ concentration leads to arsenic accumulation, weight loss, and memory impairment in mice.

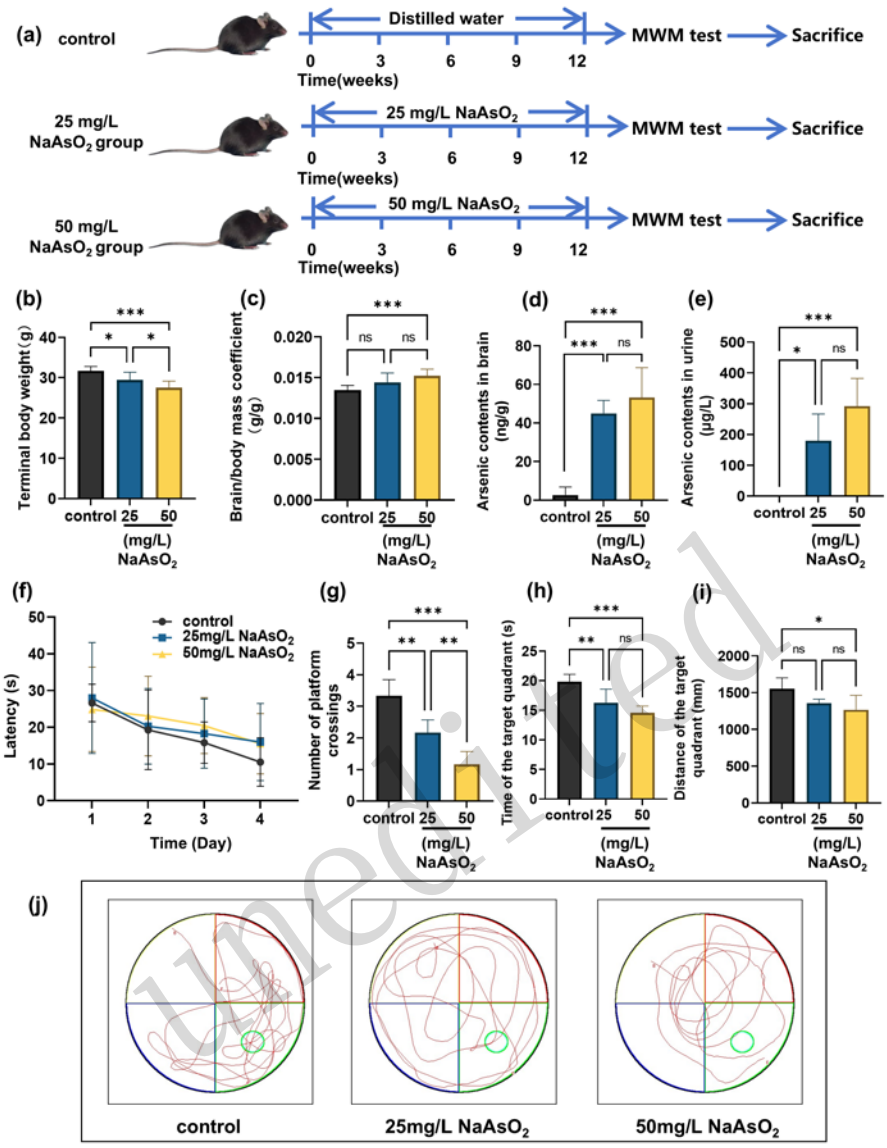

Fig. 1 Effects of $NaAsO_2$ on brain-to-body ratio and cognitive performance in mice

(a) Schematic diagram of the animal experimental design. (b) Final weight of each group of mice, n=10. (c) Changes in brain/body ratio of mice in each group, n=10. (d) Total arsenic content in the brain tissue of each group of mice, n=10. (e) Total arsenic level in the urine of each group of mice, n=4. (f) Mean escape to platform latency was recorded during the first 4 days of the morris water maze (MWM) navigation experience, n=10. (g) The number of times mice in each group crossed the platform, n=10. (h) The time mice in each group stayed in the target quadrant, n=10. (i) The distance mice in each group moved in the target quadrant, n=10. (j) Representative trajectories for space exploration testing. The values are expressed as mean±standar deviation (SD). * $P < 0.05$, ** $P < 0.01$ and *** $P < 0.001$ vs. control group or 25 mg/L $NaAsO_2$ group. ns: no significance.

3.2 Apoptosis of hippocampal neurons induced by $NaAsO_2$

In order to elucidate the effects of arsenic exposure on the structure and apoptosis of hippocampal neurons, we analyzed the pathological changes and apoptotic characteristics of mouse hippocampal tissues through H&E

staining, Nissl staining, TUNEL apoptosis assay, and TEM observation. The H&E staining revealed that the cells in the CA1 and CA3 regions of the hippocampi of control mice were tightly arranged with blue nuclei, whereas the cells of mice treated with 25 mg/L and 50 mg/L $NaAsO_2$ exhibited irregular arrangements, blurred shape and a reduced number of cells (Fig. 2a). Compared to the control mice, the Nissl positive cell counts in the hippocampal CA3 region of mice treated with 25 mg/L $NaAsO_2$ and in the hippocampal DG region in those treated with 50 mg/L $NaAsO_2$ were significantly reduced (P<0.05; Figs. 2b and 2c). Compared with that in the control mice, the apoptosis rate of hippocampal CA1 cells in the 50 mg/L $NaAsO_2$ group was significantly increased (P<0.01; Figs. 2d and 2e). The TEM results (Fig. 2f) showed that control mice exhibited intact nuclear membranes and chromatin aggregation. In contrast, mice treated with 25 mg/L $NaAsO_2$ displayed increased lipofuscin accumulation and mitochondrial swelling. More severe ultrastructural changes, including organelle depletion and nuclear membrane disruption, were observed in response to 50 mg/L $NaAsO_2$ treatment, indicating that $NaAsO_2$ causes apoptosis and ultrastructural damage in the hippocampal neurons of mice.

In addition, it was found that both 2 and 4 μmol/L $NaAsO_2$ significantly reduced HT-22 cell viability in the hippocampal neurons of mice (P<0.01 and P<0.001; Fig. 2g), with a reduction of 25% and 60%, respectively. Meanwhile, the cleaved-caspase3/caspase3 ratio in the HT-22 cells of mice treated with 4 μmol/L $NaAsO_2$ was significantly elevated compared to the control group (P<0.01; Figs. 2h and 2i). Moreover, both late-stage and total apoptosis rates of HT-22 cells exposed to 2 and 4 μmol/L $NaAsO_2$ were significantly higher than those in the control cells (P<0.01; Figs. 2j-2l). These results suggest that $NaAsO_2$ exposure significantly induces apoptosis in HT-22 cells.

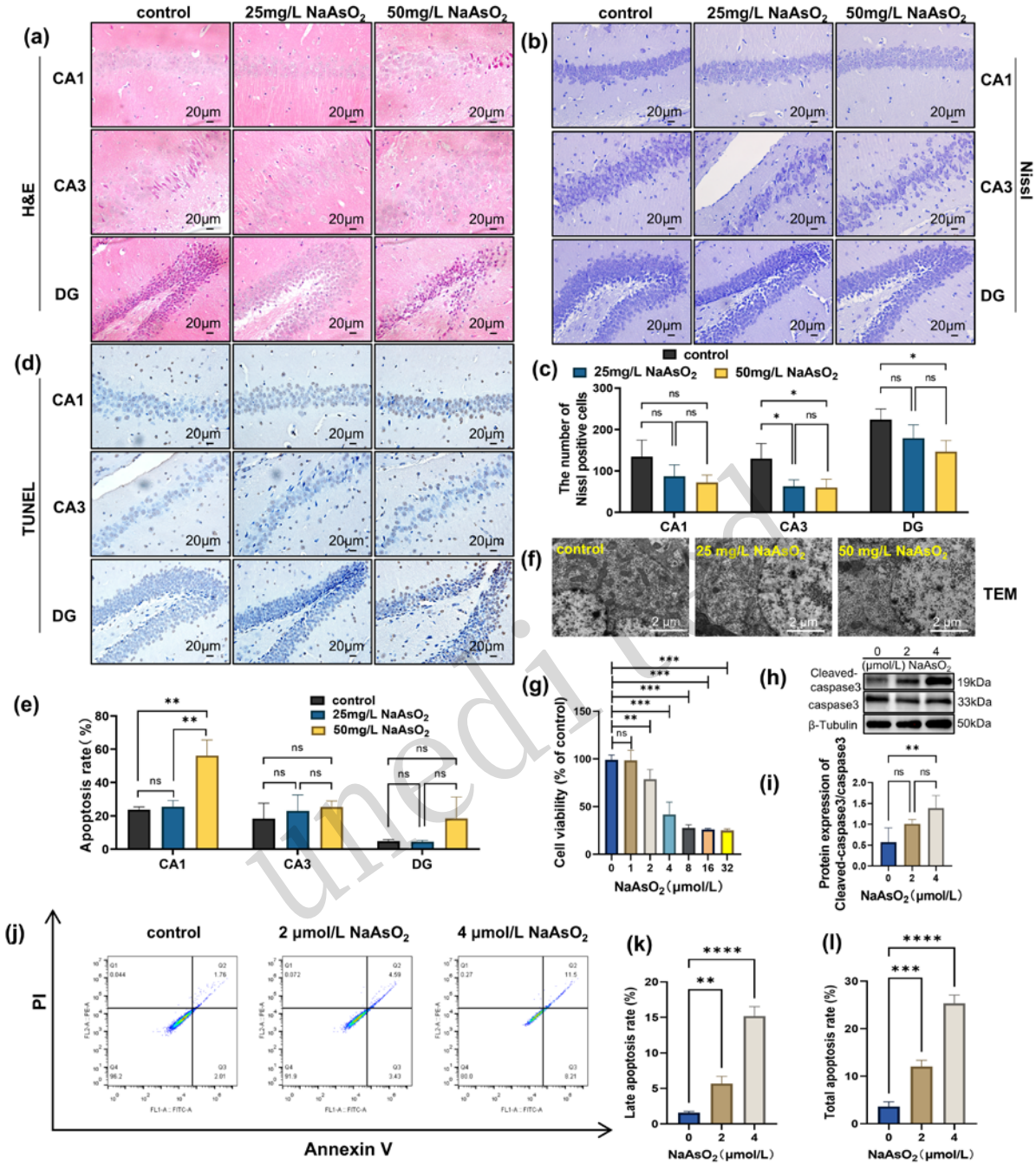

Fig. 2 $NaAsO_2$ induced structural abnormalities and apoptosis of hippocampal neurons

(a) Hematoxylin and eosin (H&E) staining of various regions in the hippocampus of mice, n=5. (b) Representative images of Nissl staining in various regions of the hippocampus (magnification 400×). (c) Dark purple staining is considered a normal Nissl body structure, and the number of Nissl positive cells represents the analysis results, n=3. (d) Representative images of terminal deoxynucleotidyl transferase dUTP nick-end labeling (TUNEL)-positive cells in various hippocampus regions (magnification 400×), with yellow brown stained nuclei considered TUNEL-positive nuclei. (e) Apoptosis rates in various regions of the hippocampus, expressed as a percentage of TUNEL-positive cells to the total number of cells, n=3. (f) Transmission electron microscopy (TEM)

was used to observe the ultrastructure of hippocampal neurons in mice (Scale bar = 2 μm). (g) Effect of $NaAsO_2$ on the viability of HT-22 cells, n=3. (h-i) Western blot analysis of the protein abundance of cleaved-caspase/caspase3 ratio, n=3. (j) Representative image of flow cytometry with Annexin V/PI staining. (k) Changes in the late apoptosis rate in different groups, n=3. (l) Changes in the total apoptosis rate in different groups, n=3. The values are expressed as mean±standar deviation (SD). * $P < 0.05$, ** $P < 0.01$, *** $P < 0.001$ and **** $P < 0.0001$. ns: no significance.

3.3 Mitochondrial dynamics imbalance in hippocampal neurons induced by $NaAsO_2$

In order to reveal the effect of arsenic exposure on mitochondrial structure and dynamics, TEM observation and protein expression analysis were performed. As shown in Fig. 3a, control HT-22 cells contained more normal mitochondria with intact structures than HT-22 cells treated with 2 and 4 μmol/L $NaAsO_2$, which were swollen and structurally abnormal. Further statistical analysis of the mitochondrial aspect ratio and morphology within the TEM field of view revealed that the mitochondrial aspect ratio in the 4 μmol/L $NaAsO_2$ group was significantly decreased, while the proportion of swollen mitochondria in the total number of mitochondria was significantly increased (P<0.05; Figs. 3b and 3c).

Notably, p-Drp1 levels in the hippocampal CA1 and CA3 regions of mice treated with 25 mg/L and 50 mg/L $NaAsO_2$ were significantly lower than those in the control mice (P<0.05; Figs. 3d and 3f). Additionally, Drp1 levels in the hippocampal CA1 region of 50 mg/L $NaAsO_2$-treated mice were significantly decreased compared to the control group (P<0.05; Figs. 3e and S1c). The p-Drp1/Drp1 ratio in the hippocampal CA1 region of $NaAsO_2$-treated mice was also significantly lower than those in the control group (P<0.05; Fig. 3g). Similarly, in the HT-22 cells treated with 4 μmol/L $NaAsO_2$, both p-Drp1 and p-Drp1/Drp1 ratio were significantly reduced compared to the control cells (P<0.01 and P<0.05; Figs. 3h-3j). Although Drp1 levels in HT-22 cells treated with 4 μmol/L $NaAsO_2$ showed a decreasing trend, the difference was not statistically significant (Fig. S1d). The expression of OPA1 in the 4 μmol/L $NaAsO_2$-treated HT-22 cells was significantly lower than that in the control cells (P<0.05; Figs. 3k-3l).

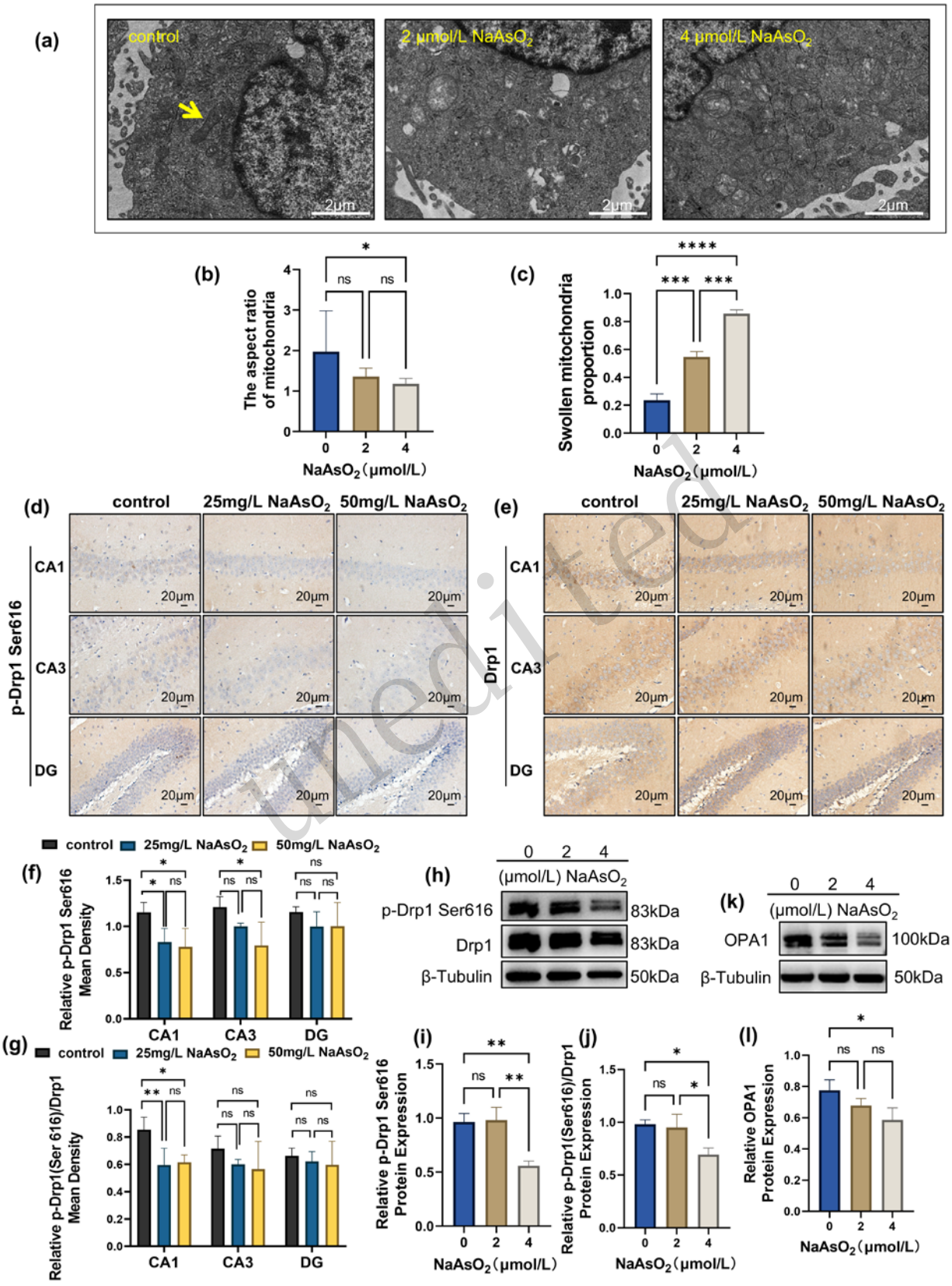

Fig. 3 $NaAsO_2$ induces mitochondrial dynamics imbalance in hippocampal neurons

(a) Transmission electron microscopy (TEM) was used to observe the morphology of mitochondria in HT-22 cells (yellow arrow: mitochondria with typical morphological characteristics, scale bar=2 μm). (b) Analysis of mitochondrial aspect ratio in TEM images for each group. n=3. (c) Ratio of the number of swollen mitochondria to the total number of mitochondria in TEM images for each group. n=3. Immunohistochemistry was used to detect representative images of (d) phosphorylated dynamin-related protein 1 (p-Drp1) Ser616 and (e) dynamin-related protein 1 (Drp1) in various regions of the hippocampus (magnification 400×). Average optical density values of (f) p-Drp1 Ser616 and (g) p-Drp1(Ser616)/Drp1 ratio in the hippocampus, n=4. (h-l) Western blot analysis of the protein abundance of p-Drp1 Ser616, p-Drp1(Ser616)/Drp1 ratio and optic atrophy 1 (OPA1). n=3. The values are expressed as mean±standar deviation (SD). * P< 0.05, ** P < 0.01, *** P < 0.001 and **** P < 0.0001. ns: no significance.

3.4 $NaAsO_2$-induced NGF decrease and NGF overexpression-mediated reduction of $NaAsO_2$-induced cell apoptosis

In order to verify whether NGF downregulation is involved in arsenic-induced neuronal damage, we detected NGF expression in the hippocampus of mice and HT-22 cells after $NaAsO_2$ treatment and evaluated the neuroprotective effect of NGF through NGF overexpression experiments. As shown in Figs. 4a-4b, NGF in the hippocampal CA1 and CA3 regions of both $NaAsO_2$-treated mice were significantly lower than those in the control group (P<0.01 and P<0.001). A similar trend was observed in the $NaAsO_2$-treated HT-22 cells, as shown by immunofluorescence (Fig. 4c). Furthermore, the results of western blot confirmed that the levels of NGF in HT-22 cells treated with 2 and 4 μmol/L $NaAsO_2$ were significantly lower than those in the control cells (P<0.05 and P<0.01; Figs. 4d and 4e).

When NGF was overexpressed in HT-22 cells via transfection with an NGF lentivirus vector (Figs. 4f and 4g), the $NaAsO_2$-induced decrease in cell viability and increase in cleaved-caspase3/caspase3 ratio were substantially alleviated (P<0.01; Figs. 4h-4j). More importantly, the late-stage and total apoptosis rates of $NaAsO_2$-treated HT-22 cells overexpressing NGF were significantly reduced compared to those of $NaAsO_2$-treated HT-22 cells (P<0.001; Figs. 4k-4m). These results indicate that NGF overexpression mitigates the arsenic-induced apoptosis of HT-22 cells.

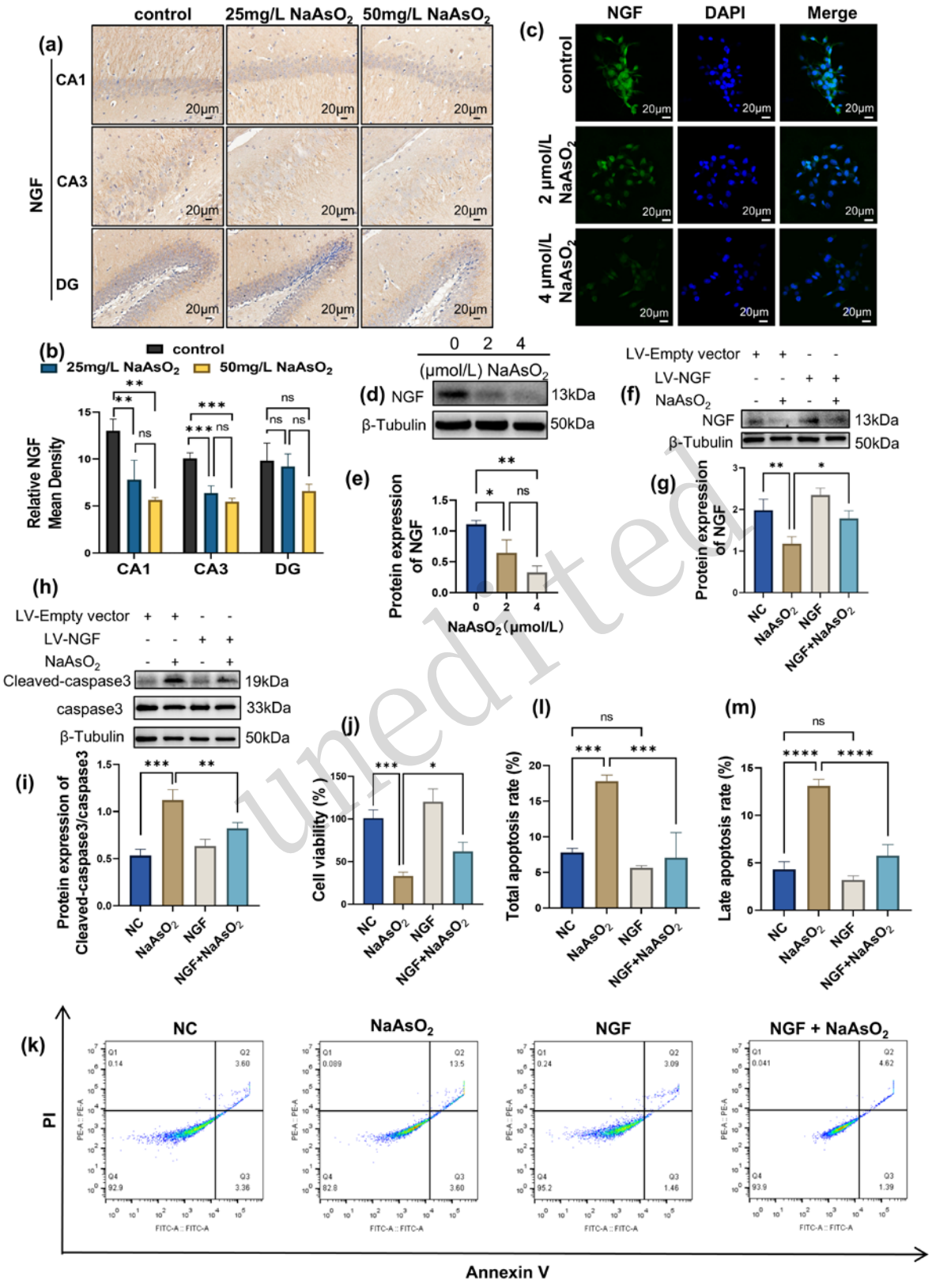

Fig. 4 Overexpression of NGF reduces $NaAsO_2$-induced cell apoptosis

(a) Immunohistochemistry was used to detect representative images of nerve growth factor (NGF) in various regions of the hippocampus (magnification 400×). (b) Average optical density values of NGF in the hippocampus, n=4. (c) The NGF fluorescence intensity in HT-22 cells treated with 2 and 4 μmol/L $NaAsO_2$ was observed using confocal microscopy (magnification 200×), n=3. (d-e) Western blot analysis of the protein abundance of NGF, n=3. Western blot analysis of (f-g) NGF and (h-i) cleaved-caspase3 expression, n=3. (j) Effect of $NaAsO_2$ on the viability of HT-22 cells after overexpression of NGF, n=3. (k) Representative image of flow cytometry with Annexin V/PI staining. (l) Changes of total apoptosis rate in different groups, n=3. (m) Changes of late apoptosis rate in different groups, n=3. The values are expressed as mean±standar deviation (SD). * $P < 0.05$, ** $P < 0.01$, *** $P < 0.001$ and **** $P < 0.0001$. ns: no significance.

3.5 Amelioration of $NaAsO_2$-induced mitochondrial dynamics imbalance via NGF overexpression

In order to verify whether NGF exerts neuroprotective effects by regulating mitochondrial dynamics, NGF was overexpressed in $NaAsO_2$-treated HT-22 cells and we further observed the changes in mitochondrial morphology, dynamics-related proteins, and cell apoptosis. As shown in Fig. 5a, NGF overexpression in HT-22 cells significantly counteracted the $NaAsO_2$-induced mitochondrial swelling and restored more mitochondria with normal morphological characteristics. Further analysis showed that NGF overexpression significantly reversed the decrease in mitochondrial aspect ratio and the increase in the proportion of swollen mitochondria in the total number of mitochondria in the $NaAsO_2$ group ($P<0.05$; Figs. 5b and 5c). Additionally, NGF overexpression significantly reversed $NaAsO_2$-induced reductions in p-Drp1, p-Drp1/Drp1, and OPA1 levels ($P<0.05$; Figs. 5d-5h), while the changes in Drp1 levels were not statistically significant (Fig. S1e). Immunofluorescence analysis further corroborated these findings, showing that NGF overexpression significantly restored p-Drp1 and OPA1 levels (Figs. 5i and 5j), whereas Drp1 levels remained unchanged (Fig. S1f). These results suggest that NGF overexpression mitigates the $NaAsO_2$-induced imbalance of mitochondrial dynamics.

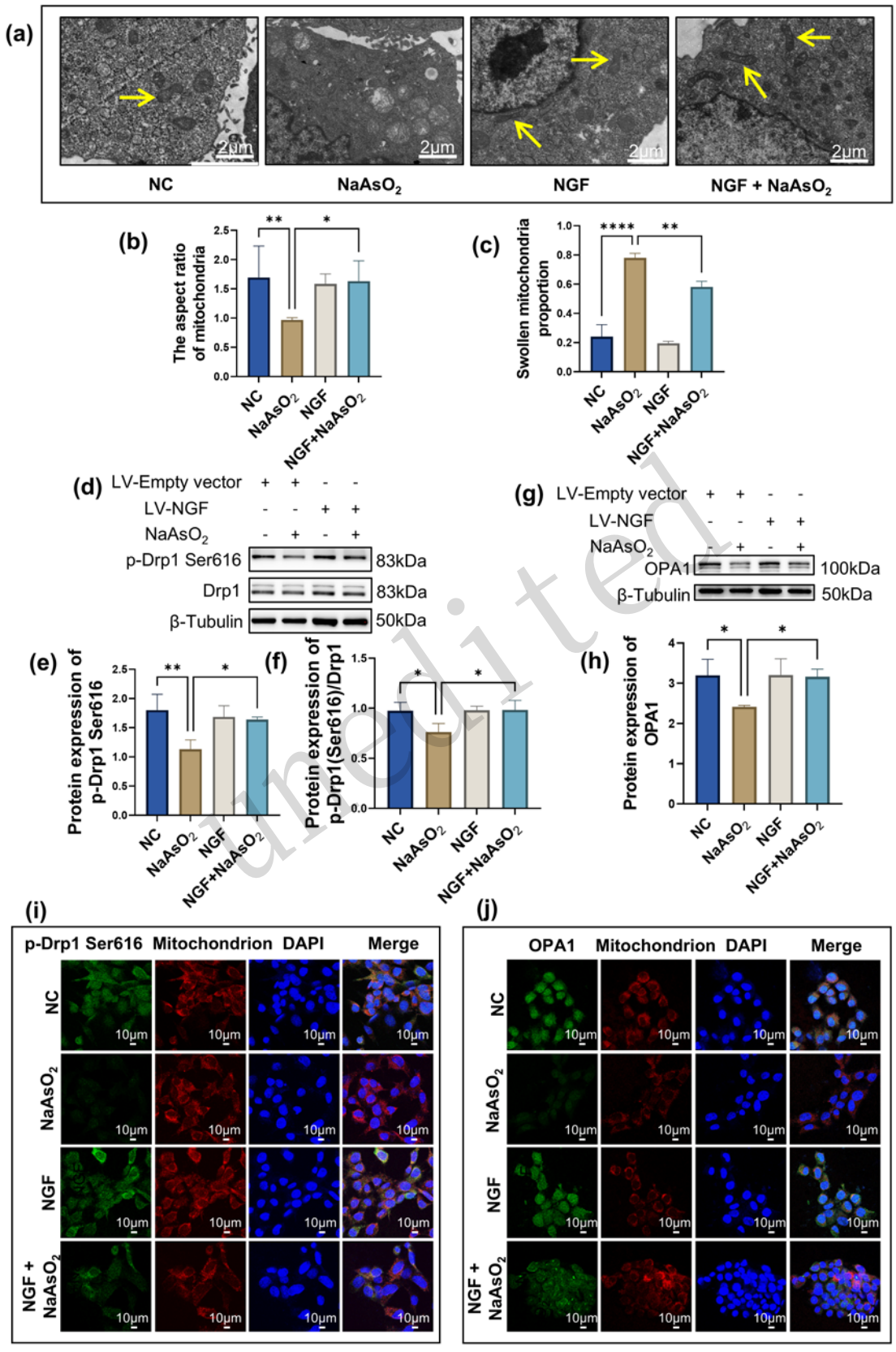

Fig. 5 Overexpression of NGF improves mitochondrial dynamics imbalance caused by $NaAsO_2$

(a) Transmission electron microscopy (TEM) was used to observe the morphology of mitochondria in HT-22 cells (yellow arrow: mitochondria with typical morphological characteristics, scale bar=2 μm). (b) Analysis of mitochondrial aspect ratio in TEM images for each group. n=3. (c) Ratio of the number of swollen mitochondria to the total number of mitochondria in TEM images for each group. n=3. (d-f) Western blot analysis of the protein abundance of phosphorylated dynamin-related protein 1 (p-Drp1) Ser616 and p-Drp1(Ser616)/dynamin-related protein 1 (Drp1). n=3. (g-h) Western Blot analysis of the protein abundance of optic atrophy 1 (OPA1), n=3. (i) The p-Drp1 Ser616 and (j) OPA1 fluorescence intensity in HT-22 cells were observed using confocal microscopy (scale bar=10 μm), n=3. The values are expressed as mean±standar deviation (SD). * $P < 0.05$, ** $P < 0.01$ and **** $P < 0.0001$.

3.6 Attenuation of arsenic-induced effects on PI3K/AKT signaling pathways by NGF

In order to clarify whether NGF-mediated neuroprotection depends on the PI3K/AKT signaling pathway, we detected the phosphorylation levels of PI3K/AKT and the expression of downstream molecule ATP dependent metalloprotease (YME1L1) in the hippocampus of mice and cells after arsenic exposure and analyzed the regulatory effect of NGF on this pathway. The YME1L1 levels in the mice hippocampus exposed to 50 mg/L $NaAsO_2$ group were significantly lower than those in the control group ($P<0.001$; Figs. 6a and 6b), and 4 μmol/L $NaAsO_2$ significantly reduced YME1L1 in HT-22 cells compared to the control group ($P<0.01$; Figs. 6c and 6d). As shown in Figs. 6e-6h and S2a-S2b, p-AKT/AKT in CA3 and DG regions of mouse hippocampi in the 50 mg/L $NaAsO_2$ group was significantly lower than that in the control group ($P<0.05$ and $P<0.001$). Although p-PI3K/PI3K was also reduced, the difference was not statistically significant. The western blot results (Figs. 6i-6l) revealed that p-PI3K/PI3K and p-AKT/AKT levels in HT-22 cells treated with 4 μmol/L $NaAsO_2$ were significantly lower than those in the control group ($P<0.05$).

NGF overexpression reversed the reduction in YME1L1, p-PI3K/PI3K and p-AKT/AKT caused by 4 μmol/L $NaAsO_2$ ($P<0.05$; Figs. 6m-6p). These results indicate that NGF attenuates arsenic-induced disruptions in PI3K/AKT-related signaling pathways.

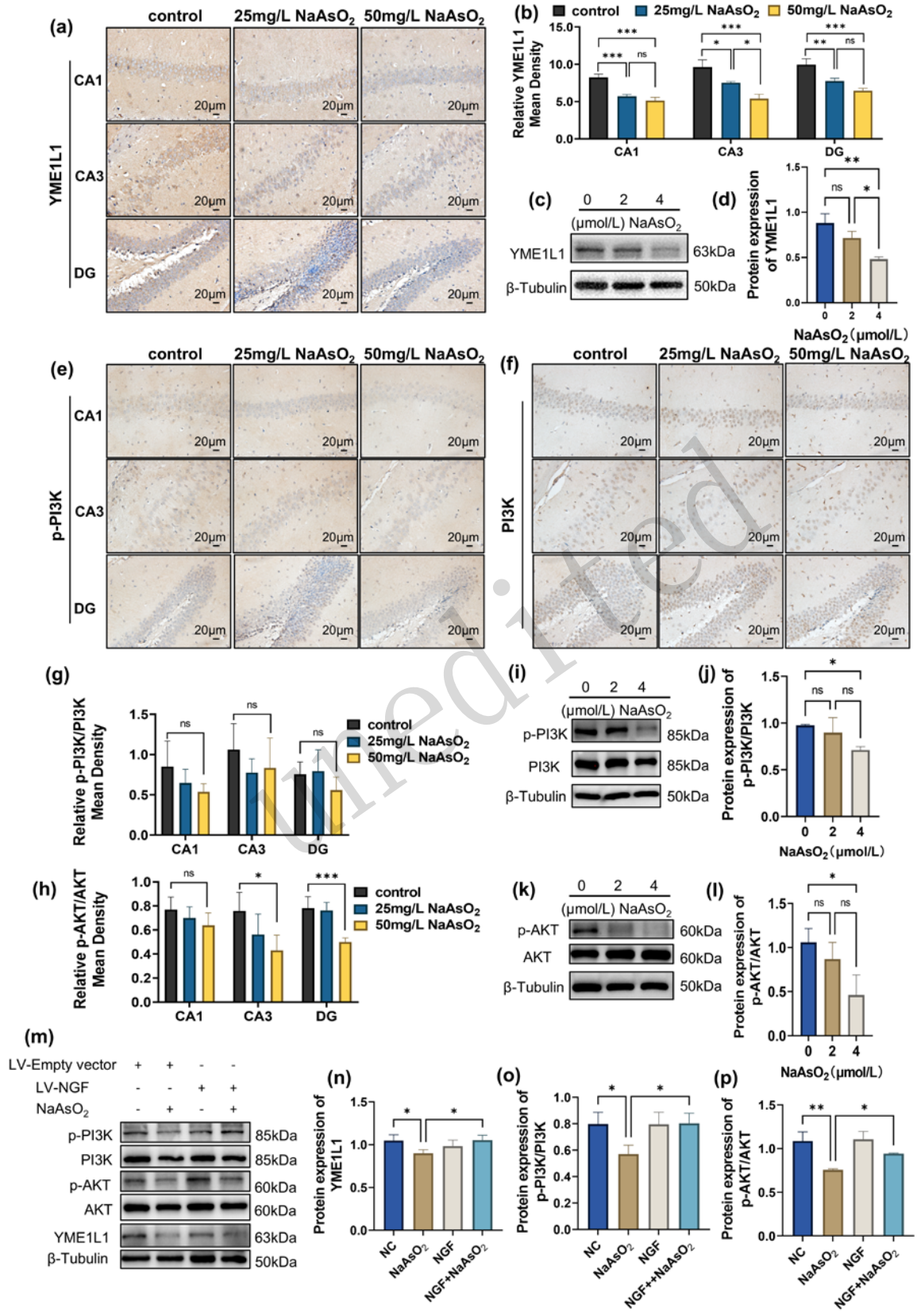

Fig. 6 NGF attenuates the effects of arsenic on PI3K/AKT-related signaling pathways

Immunohistochemistry was used to detect representative images of (a) ATP dependent metalloprotease (YME1L1), (e) phosphorylation of phosphatidylinositol 3-kinase (p-PI3K) and (f) phosphatidylinositol 3-kinase (PI3K) in various regions of the hippocampus (magnification 400×). Average optical density values of (b) YME1L1, (g) p-PI3K/PI3K and (h) phosphorylation of protein kinase B (p-AKT)/protein kinase B (AKT) in the hippocampus, n=3. (c-d) YME1L1, (i-j) p-PI3K/PI3K and (k-l) p-AKT/AKT protein in HT-22 cells treated by $NaAsO_2$ were detected by western blot. (m-p) Immunoblotting was used to detect the protein content of YME1L1, p-PI3K/PI3K and p-AKT/AKT in HT-22 cells overexpressing nerve growth factor (NGF). The values are expressed as mean±standar deviation (SD). * P< 0.05, ** P < 0.01 and *** P < 0.001. ns: no significance.

3.7 Inhibition of PI3K/AKT signaling pathway-mediated weakening of NGF's protective effect on arsenic exposure-caused mitochondrial dynamics imbalance

In order to verify the necessity of the PI3K/AKT pathway in NGF-regulated mitochondrial dynamics, we inhibited this pathway using LY294002 and subsequently analyzed the signaling-dependent mechanism of NGF's protective effect by detecting the expression of mitochondrial-related proteins and the cell apoptosis rate. As shown in Figs. 7a-7g, treatment with 20 μmol/L LY294002 significantly attenuated the protective effect of NGF overexpression on apoptosis in HT-22 cells and reduced the impact of arsenic exposure on the PI3K/AKT signaling pathway. Specifically, compared with the LV-NGF + $NaAsO_2$ group, the LV-NGF + $NaAsO_2$ + LY294002 group exhibited a significant increase in cleaved-caspase3/caspase3 in HT-22 cells (P<0.05), while p-PI3K/PI3K, p-AKT/AKT and YME1L1 were significantly decreased (P<0.001, P<0.05 and P<0.05).

Compared with the LV-NGF + $NaAsO_2$ group, LY294002 significantly weakened the protective effect of NGF overexpression on the decrease of p-Drp1, Drp1, p-Drp1/Drp1, and OPA1 in HT-22 cells caused by arsenic (P<0.001, P<0.05, P<0.05, and P<0.05, respectively; Figs. 7h-7l and S2c). Flow cytometry analysis demonstrated that, compared to HT-22 cells in the LV-NGF + $NaAsO_2$ group, those in the LV-NGF + $NaAsO_2$ + LY294002 group had significantly increased total and late apoptosis rates (P<0.01 and P<0.001; Figs. 7m-7o). These findings indicate that LY294002 significantly reduces the inhibitory effects of NGF overexpression on arsenic-induced apoptosis in HT-22 cells.

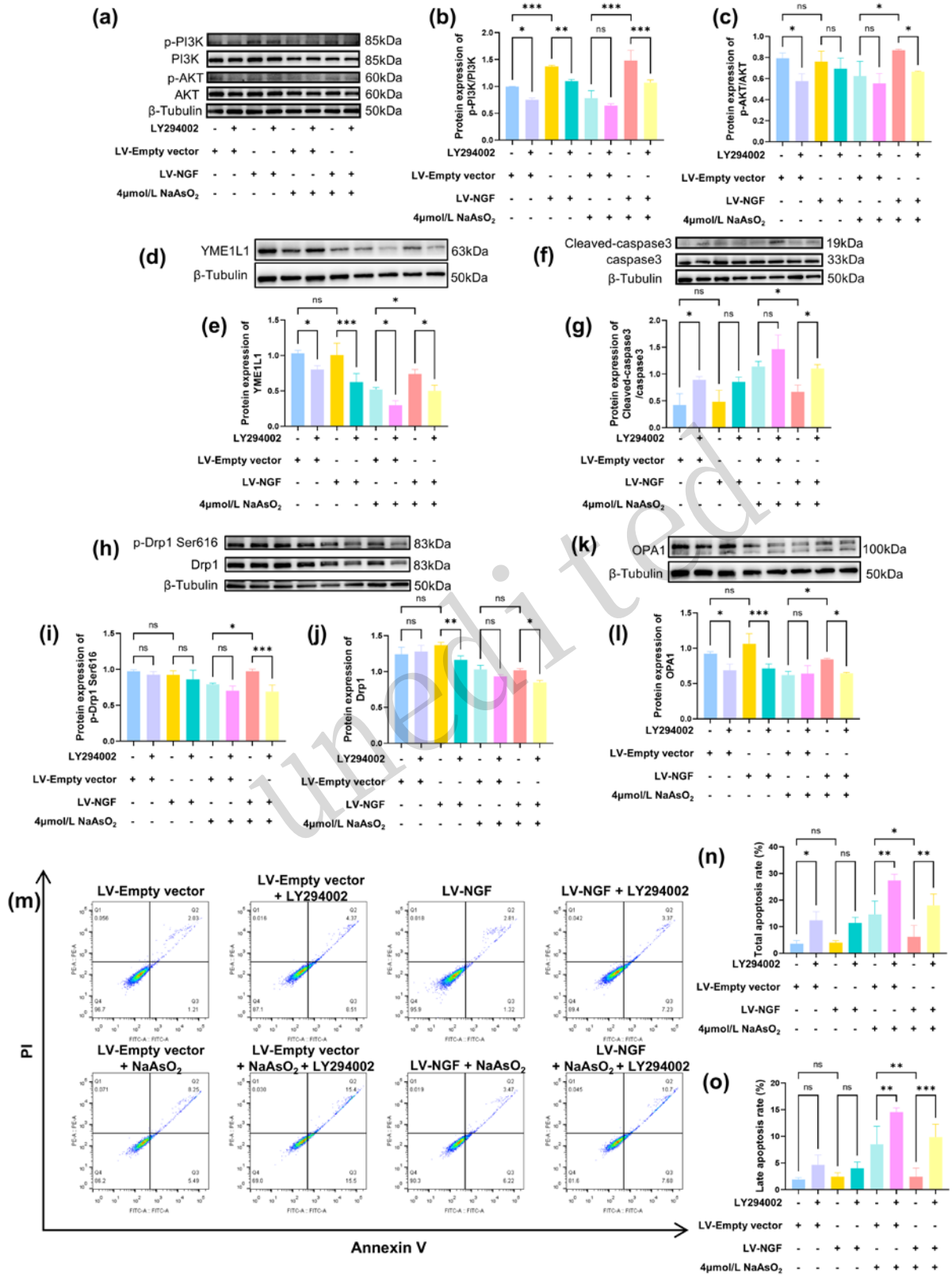

Fig. 7 Inhibition of the PI3K/AKT signaling pathway can weaken the protective effect of NGF on mitochondrial dynamics

(a-c) phosphorylation of phosphatidylinositol 3-kinase (p-PI3K)/phosphatidylinositol 3-kinase (PI3K), phosphorylation of protein kinase B (p-AKT)/protein kinase B (AKT), (d-e) ATP dependent metalloprotease (YME1L1), (f-g) cleaved-caspase3, (h-j) p-Drp1 Ser616, Drp1 and (k-l) YME1L1 protein in HT-22 cells treated by LY294002 were detected by western blot, n=3. (m) Representative image of flow cytometry with Annexin V/PI staining. (n) Changes in the total apoptosis rate in different groups, n=3. (o) Changes in the late apoptosis rate in different groups, n=3. The values are expressed as mean±standar deviation (SD). * $P < 0.05$, ** $P < 0.01$ and *** $P < 0.001$. ns: no significance.

4 Discussion

Studies have established that serum NGF is positively correlated with cognitive ability scores and NGF supplementation can improve cognitive function in patients (Olson, 1993; He et al., 2024). This has sparked our interest in exploring the role of NGF reduction in arsenic-induced cognitive impairment. Four-week-old mice correspond to human adolescence, during which the nervous system remains in a developmental stage (Kang et al., 2024). Arsenic exhibits more significant toxicity during this period, particularly affecting growth and development, metabolic homeostasis, and poses long-term health risks (Tolins et al., 2014). Our previous study (Lv, et al., 2023) found that 25 mg/L and 50 mg/L $NaAsO_2$ could induce neural damage in 4-week-old mice. Therefore, in this study, we established a model of 4-week-old male mice treated with 25 mg/L and 50 mg/L $NaAsO_2$.

In our animal experiments, $NaAsO_2$ significantly inhibited the expression of NGF, accompanied by impaired learning and memory abilities, reduced hippocampal neurons, and increased cell apoptosis rate in mice. These findings indicate that our animal model was successfully established. Notably, although there was no significant difference in the brain arsenic and urine arsenic levels between the 25 mg/L and 50 mg/L groups, both brain arsenic (R=0.82, P<0.05) and urine arsenic (R=0.89, P<0.05) levels showed a significant positive correlation with the arsenic exposure dose. Indeed, the 50 mg/L group exhibited more pronounced effects on certain outcomes, such as body weight reduction, MWM performance, loss of Nissl-stained positive cells, and CA1 apoptosis. It has been reported that CA1 neurons are more susceptible to arsenic due to their higher energy demand (Wang and Michaelis, 2010), which may explain why the apoptosis rate in the CA1 region was significantly higher than that in the control group. Following treatment with 50 mg/L $NaAsO_2$, the number of Nissl-positive cells in the hippocampal CA3 and DG regions was significantly lower than that in the control group, with no corresponding increase in apoptosis rates; in contrast, elevated apoptosis was exclusively observed in the CA1 region. TUNEL positivity specifically reflects apoptotic events, while Nissl staining primarily reveals large-scale cell loss resulting from apoptosis, necrosis, or non-apoptotic cell death. Therefore, these findings suggest that non-apoptotic cell death pathways may more prominently mediate arsenic-induced loss of Nissl-positive cells in the hippocampal CA3 and DG regions. Notably, *in vitro* studies further confirmed that $NaAsO_2$ induces apoptosis and ultrastructural damage in HT-22 cells. NGF is widely recognized as a key regulator of neural function and its downregulation may contribute to neuronal damage and cognitive impairment. Importantly, NGF treatment has been shown to improve cognitive function (Lu et al., 2023a). Thus, we hypothesized that reduced NGF levels are a key factor in arsenic-induced neurotoxicity. It is well-known that the regulatory mechanisms of NGF expression involve multiple factors, such as oxidative stress, epigenetic modifications, and non-coding RNAs (Heberlein et al., 2013; Tsai et al., 2014), thereby the specific mechanisms by which arsenic affects NGF levels remain to be further investigated.

Studies have highlighted that NGF enhances mitochondrial dynamics by upregulating mitochondrial fusion- and fission-related proteins, thereby promoting normal neuronal differentiation (Martorana, et al., 2018; Goglia et al., 2024). Drp1 is a key regulator of mitochondrial fission, and p-Drp1 modulates the

localization and aggregation of Drp1 in mitochondria, affecting the process of mitochondrial fission (Schmitt et al., 2018; Gao et al., 2022b). OPA1, located in the inner mitochondrial membrane, plays a crucial role in maintaining the structure of mitochondrial cristae and genome stability (Frezza et al., 2006). The interaction and balance of these fusion- and fission-related proteins are essential for mitochondria integrity and function. Under pathological conditions, a dysregulation of p-Drp1, Drp1 and OPA1 may lead to mitochondrial dysfunction, resulting in cell death and tissue damage (Qin and Xi, 2022). Francesca Martorana et al. found that NGF-induced neuronal differentiation is accompanied by increased mitochondrial remodeling, as evidenced by the upregulation of p-Drp1 and OPA1 (Martorana, et al., 2018). Our results indicate that $NaAsO_2$ significantly disrupts mitochondrial fusion and fission, leading to mitochondrial swelling and cristae dissipation. We hypothesized that arsenic-induced mitochondrial alterations may be linked to the dysregulation of mitochondrial dynamics-related proteins, including p-Drp1, Drp1 and OPA1. Consistent with this hypothesis, the levels of mitochondrial fission-related proteins p-Drp1/Drp1 and fusion protein OPA1 were significantly reduced in arsenic-treated mice and HT-22 cells. Previous studies have shown that the protection of damaged neurons by stimulating NGF release is associated with the activation of PI3K/AKT cell survival signaling (Sang et al., 2018). Combined with the findings of this study, the protective effect of NGF on neurons may be related to its alleviation of mitochondrial dynamic imbalance via the PI3K/AKT pathway. Therefore, we speculate that arsenic can further inhibit p-Drp1 and OPA1 by reducing NGF, thereby damaging mitochondrial dynamics and ultimately leading to neurotoxicity.

The PI3K/AKT pathway has been shown to regulate the phosphorylation level of Drp1 and the level of OPA1 to maintain mitochondrial homeostasis and normal function (Kim et al., 2016; Wang et al., 2023). In the present study, $NaAsO_2$ significantly reduced the levels of p-PI3K/PI3K and p-AKT/AKT in the hippocampal tissue of mice and HT-22 cells, indicating that $NaAsO_2$ can inactivate the PI3K/AKT signaling pathway, consistent with previous reports (Goussetis and Platanias, 2010). Further research has shown that NGF overexpression alleviates the inhibitory effect of arsenic on AKT activation. In addition, arsenic exposure significantly reduced the expression of YME1L1, a lytic enzyme involved in OPA1 activation, whose deficiency leads to cell proliferation defects and mitochondrial fusion disorders (Hartmann et al., 2016). Our research suggests that arsenic suppresses mitochondrial fusion by inhibiting PI3K/AKT phosphorylation via NGF reduction, which may be related to the reduction in YME1L1. Previous studies have shown that NGF activates PI3K/AKT cell survival signaling to promote neuronal survival and enhance mitochondrial length and density (Sang, et al., 2018; Armijo-Weingart et al., 2019). In our study, LY294002, an inhibitor of the PI3K/AKT signaling pathway, significantly antagonized the protective effects of NGF on p-Drp1, Drp1, OPA1, and cell viability. These findings suggest that arsenic-induced NGF reduction inhibits mitochondrial dynamics via the PI3K/AKT pathway, ultimately leading to cognitive impairment. It is worth noting that NGF exerts its effects by binding to its receptor TrkA and may also influence neuronal survival through alternative pathways, such as PLC-γ (Huang and Reichardt, 2003; Calvo-Enrique et al., 2023). Future genetic intervention studies targeting TrkA and PLC-γ are necessary to further elucidate these mechanisms.

5 Conclusions

Arsenic-induced cognitive impairment and neuronal damage were found to be associated with NGF downregulation and mitochondrial dynamics imbalance. Furthermore, NGF supplementation mitigated these effects, with the PI3K/AKT pathway playing a crucial role in the neuroprotective response to arsenic exposure. These findings provide novel insights into the mechanisms underlying arsenic-induced neurotoxicity and suggest that

NGF-mediated mitochondrial regulation may serve as a potential therapeutic target for arsenic-related neurological disorders.

Data availability statement

The datasets used and analyzed during the current study are available from the corresponding author on reasonable request.

Acknowledgments

This work was supported by the HMU Marshal Initiative Funding (Grant number HMUMIF-21014).

Author contributions

Xinbo MA: Methodology, Writing—original draft, Software. **Liu YANG:** Writing—review and editing. **Xinhua SHAO:** Methodology. **Jia CUI:** Methodology. **Ziqiao GUAN:** Methodology. **Man LV:** Methodology. **Shuaifei YANG:** Methodology. **Na FANG:** Methodology. **Yang LIU:** Methodology. **Yanhui GAO:** Conceptualization. **Xiaona LIU:** Conceptualization, Writing—review and editing, Funding acquisition. **Yanmei YANG:** Conceptualization, Writing—review and editing, Data curation, Funding acquisition.

Compliance with ethics guidelines

The authors have declared that no competing interest exists.

Animal experimentation (HRBMUECDC20210902) was approved by the Ethics Committee of the Center for Endemic Disease Control, Chinese Center for Disease Control and Prevention, Harbin Medical University. The proof or certificate of approval can be furnished upon request.

References

Armijo-Weingart L, Ketschek A, Sainath R, et al., 2019. Neurotrophins induce fission of mitochondria along embryonic sensory axons. *Elife*, 8:e49494. https://doi.org/10.7554/eLife.49494

Baruch-Eliyahu N, Rud V, Braiman A, et al., 2019. Telomerase increasing compound protects hippocampal neurons from amyloid beta toxicity by enhancing the expression of neurotrophins and plasticity related genes. *Sci Rep*, 9(1):18118. https://doi.org/10.1038/s41598-019-54741-7

Bertholet AM, Delerue T, Millet AM, et al., 2016. Mitochondrial fusion/fission dynamics in neurodegeneration and neuronal plasticity. *Neurobiol Dis*, 90:3-19. https://doi.org/10.1016/j.nbd.2015.10.011

Bozack AK, Hall MN, Liu X, et al., 2019. Folic acid supplementation enhances arsenic methylation: Results from a folic acid and creatine supplementation randomized controlled trial in bangladesh. *Am J Clin Nutr*, 109(2):380-391. https://doi.org/10.1093/ajcn/nqy148

Calvo-Enrique L, Lisa S, Vicente-Garcia C, et al., 2023. Enhanced trka signaling impairs basal forebrain-dependent behavior. *Front Mol Neurosci*, 16:1266983. https://doi.org/10.3389/fnmol.2023.1266983

Chen W, Zhao HK, Li YS, 2023. Mitochondrial dynamics in health and disease: Mechanisms and potential targets. *Signal Transduct Target Ther*, 8(1):333. https://doi.org/10.1038/s41392-023-01547-9

Cho HK, Kim W, Lee KY, et al., 2020. Beta-nerve growth factor gene therapy alleviates pyridoxine-induced neuropathic damage by increasing doublecortin and tyrosine kinase a in the dorsal root ganglion. *Neural Regen Res*, 15(1):162-168. https://doi.org/10.4103/1673-5374.264472

Cronican AA, Fitz NF, Carter A, et al., 2013. Genome-wide alteration of histone h3k9 acetylation pattern in mouse offspring prenatally exposed to arsenic. *PLoS One*, 8(2):e53478. https://doi.org/10.1371/journal.pone.0053478

Ding B, Ma XB, Liu Y, et al., 2023. Arsenic-induced, mitochondria-mediated apoptosis is associated with decreased peroxisome proliferator-activated receptor gamma coactivator alpha in rat brains. *Toxics*, 11(7) https://doi.org/10.3390/toxics11070576

Fei DX, Zhao HJ, Wang Y, et al., 2019. The disturbance of autophagy and apoptosis in the gizzard caused by copper and/or arsenic are related to mitochondrial kinetics. *Chemosphere*, 231:1-9. https://doi.org/10.1016/j.chemosphere.2019.05.101

Frezza C, Cipolat S, Martins De Brito O, et al., 2006. Opa1 controls apoptotic cristae remodeling independently from mitochondrial fusion. *Cell*, 126(1):177-189. https://doi.org/10.1016/j.cell.2006.06.025

Gao Q, Tian R, Han H, et al., 2022a. Pink1-mediated drp1(s616) phosphorylation modulates synaptic development and plasticity via promoting mitochondrial fission. *Signal Transduct Target Ther*, 7(1):103. https://doi.org/10.1038/s41392-022-00933-z

Gao QT, Tian RY, Han HL, et al., 2022b. Pink1-mediated drp1(s616) phosphorylation modulates synaptic development and plasticity via promoting mitochondrial fission. *Signal Transduct Target Ther*, 7(1):103.

https://doi.org/10.1038/s41392-022-00933-z
Goglia I, Weglarz-Tomczak E, Gioia C, et al., 2024. Fusion-fission-mitophagy cycling and metabolic reprogramming coordinate nerve growth factor (ngf)-dependent neuronal differentiation. *FEBS J*, 291(13):2811-2835. https://doi.org/10.1111/febs.17083
Goussetis DJ, Platanias LC, 2010. Arsenic trioxide and the phosphoinositide 3-kinase/akt pathway in chronic lymphocytic leukemia. *Clin Cancer Res*, 16(17):4311-4312. https://doi.org/10.1158/1078-0432.CCR-10-1496
Hartmann B, Wai T, Hu H, et al., 2016. Homozygous yme1l1 mutation causes mitochondriopathy with optic atrophy and mitochondrial network fragmentation. *Elife*, 5:e16078. https://doi.org/10.7554/eLife.16078
He MY, Liu Z, Lian TH, et al., 2024. Role of nerve growth factor on cognitive impairment in patients with alzheimer's disease carrying apolipoprotein e epsilon4. *CNS Neurosci Ther*, 30(6):e14560. https://doi.org/10.1111/cns.14560
Heberlein A, Muschler M, Frieling H, et al., 2013. Epigenetic down regulation of nerve growth factor during alcohol withdrawal. *Addict Biol*, 18(3):508-510. https://doi.org/10.1111/j.1369-1600.2010.00307.x
Hong YS, Song KH, Chung JY, 2014. Health effects of chronic arsenic exposure. *J Prev Med Public Health*, 47(5):245-252. https://doi.org/10.3961/jpmph.14.035
Huang EJ, Reichardt LF, 2003. Trk receptors: Roles in neuronal signal transduction. *Annu Rev Biochem*, 72:609-642. https://doi.org/10.1146/annurev.biochem.72.121801.161629
Jeong S, Ahn C, Kwon JS, et al., 2023. Effects of sodium arsenite on the myocardial differentiation in mouse embryonic bodies. *Toxics*, 11(2) https://doi.org/10.3390/toxics11020142
Ji SJ, Wu HH, Ding X, et al., 2020. Increased hippocampal trka expression ameliorates cranial radiation-induced neurogenesis impairment and cognitive deficit via pi3k/akt signaling. *Oncol Rep*, 44(6):2527-2536. https://doi.org/10.3892/or.2020.7782
Kang JY, Lee JS, Wang JH, et al., 2024. Sleep deprivation in adolescent mice impairs long-term memory till early adulthood via suppression of hippocampal astrocytes. *Sleep*, 47(10) https://doi.org/10.1093/sleep/zsae143
Kim DI, Lee KH, Gabr AA, et al., 2016. Abeta-induced drp1 phosphorylation through akt activation promotes excessive mitochondrial fission leading to neuronal apoptosis. *Biochim Biophys Acta*, 1863(11):2820-2834. https://doi.org/10.1016/j.bbamcr.2016.09.003
Lai YX, Lin PQ, Chen ML, et al., 2020. Restoration of l-opa1 alleviates acute ischemic stroke injury in rats via inhibiting neuronal apoptosis and preserving mitochondrial function. *Redox Biol*, 34:101503. https://doi.org/10.1016/j.redox.2020.101503
Liu JT, Bain LJ, 2018. Arsenic induces members of the mmu-mir-466-669 cluster which reduces neurod1 expression. *Toxicol Sci*, 162(1):64-78. https://doi.org/10.1093/toxsci/kfx241
Liu Y, Zhao H, Wang Y, et al., 2020. Arsenic (iii) and/or copper (ii) induces oxidative stress in chicken brain and subsequent effects on mitochondrial homeostasis and autophagy. *J Inorg Biochem*, 211:111201. https://doi.org/10.1016/j.jinorgbio.2020.111201
Lu CL, Li S, Kang L, et al., 2023a. Aripiprazole combined with nerve growth factor improves cognitive function in mice with schizophrenia model. *Neurosci Lett*, 812:137410. https://doi.org/10.1016/j.neulet.2023.137410
Lu H, Yin K, Su H, et al., 2023b. Polystyrene microplastics induce autophagy and apoptosis in birds lungs via pten/pi3k/akt/mtor. *Environ Toxicol*, 38(1):78-89. https://doi.org/10.1002/tox.23663
Lu H, Zhang Y, Zhang X, et al., 2024. New insights into zinc alleviating renal toxicity of arsenic-exposed carp (cyprinus carpio) through yap-tfr/ros signaling pathway. *Pestic Biochem Physiol*, 205:106153. https://doi.org/10.1016/j.pestbp.2024.106153
Lv M, Ma XB, Zhang KY, et al., 2023. The disruption of blood-brain barrier induced by long-term arsenic exposure is associated with the increase of mmp-9 and mmp-2: The characteristics are similar to those caused by senescence. *Chem Biol Interact*, 385:110743. https://doi.org/10.1016/j.cbi.2023.110743
Malewska-Kasprzak M, Skibinska M, Dmitrzak-Weglarz M, 2024. Alterations in neurotrophins in alcohol-addicted patients during alcohol withdrawal. *Brain Sci*, 14(6) https://doi.org/10.3390/brainsci14060583
Marlin MC, Li G, 2015. Biogenesis and function of the ngf/trka signaling endosome. *Int Rev Cell Mol Biol*, 314:239-257. https://doi.org/10.1016/bs.ircmb.2014.10.002
Martorana F, Gaglio D, Bianco MR, et al., 2018. Differentiation by nerve growth factor (ngf) involves mechanisms of crosstalk between energy homeostasis and mitochondrial remodeling. *Cell Death Dis*, 9(3):391. https://doi.org/10.1038/s41419-018-0429-9
Mu MY, Zhao HJ, Wang Y, et al., 2019. Arsenic trioxide or/and copper sulfate co-exposure induce glandular stomach of chicken injury via destruction of the mitochondrial dynamics and activation of apoptosis as well as autophagy. *Ecotoxicol Environ Saf*, 185:109678. https://doi.org/10.1016/j.ecoenv.2019.109678
Olson L, 1993. Ngf and the treatment of alzheimer's disease. *Exp Neurol*, 124(1):5-15. https://doi.org/10.1006/exnr.1993.1167
Peel HR, Balogun FO, Bowers CA, et al., 2022. Towards understanding factors affecting arsenic, chromium, and vanadium mobility in the subsurface. *Water (Basel)*, 14(22) https://doi.org/10.3390/w14223687
Prakash C, Soni M, Kumar V, 2016. Mitochondrial oxidative stress and dysfunction in arsenic neurotoxicity: A review. *J Appl Toxicol*, 36(2):179-188. https://doi.org/10.1002/jat.3256
Qin LY, Xi SH, 2022. The role of mitochondrial fission proteins in mitochondrial dynamics in kidney disease. *Int J Mol Sci*, 23(23):14725. https://doi.org/10.3390/ijms232314725
Sanchez-Infantes D, Cereijo R, Sebastiani G, et al., 2018. Nerve growth factor levels in term human infants: Relationship to prenatal growth and early postnatal feeding. *Int J Endocrinol*, 2018:7562702. https://doi.org/10.1155/2018/7562702

Sang QL, Sun DJ, Chen ZH, et al., 2018. Ngf and pi3k/akt signaling participate in the ventral motor neuronal protection of curcumin in sciatic nerve injury rat models. *Biomed Pharmacother*, 103:1146-1153. https://doi.org/10.1016/j.biopha.2018.04.116

Schmitt K, Grimm A, Dallmann R, et al., 2018. Circadian control of drp1 activity regulates mitochondrial dynamics and bioenergetics. *Cell Metab*, 27(3):657-666 e655. https://doi.org/10.1016/j.cmet.2018.01.011

Sevak P, Pushkar B, 2024. Arsenic pollution cycle, toxicity and sustainable remediation technologies: A comprehensive review and bibliometric analysis. *J Environ Manage*, 349:119504. https://doi.org/10.1016/j.jenvman.2023.119504

Sung KJ, Ferrari LF, Yang WL, et al., 2018. Swedish nerve growth factor mutation (ngf(r100w)) defines a role for trka and p75(ntr) in nociception. *J Neurosci*, 38(14):3394-3413. https://doi.org/10.1523/JNEUROSCI.1686-17.2018

Tan Z, Kang T, Zhang XL, et al., 2019. Nerve growth factor prevents arsenic-induced toxicity in pc12 cells through the akt/gsk-3beta/nfat pathway. *J Cell Physiol*, 234(4):4726-4738. https://doi.org/10.1002/jcp.27255

Tolins M, Ruchirawat M, Landrigan P, 2014. The developmental neurotoxicity of arsenic: Cognitive and behavioral consequences of early life exposure. *Ann Glob Health*, 80(4):303-314. https://doi.org/10.1016/j.aogh.2014.09.005

Tsai MS, Lin YC, Sun CK, et al., 2014. Up-regulation of nerve growth factor in cholestatic livers and its hepatoprotective role against oxidative stress. *PLoS One*, 9(11):e112113. https://doi.org/10.1371/journal.pone.0112113

Tuon L, Tramontin NS, Custodio I, et al., 2023. Serum biomarkers to mild cognitive deficits in children and adolescents. *Mol Neurobiol*, 60(12):7080-7087. https://doi.org/10.1007/s12035-023-03536-z

Wang X, Michaelis EK, 2010. Selective neuronal vulnerability to oxidative stress in the brain. *Front Aging Neurosci*, 2:12. https://doi.org/10.3389/fnagi.2010.00012

Wang X, Huang XY, Zhou L, et al., 2021. Association of arsenic exposure and cognitive impairment: A population-based cross-sectional study in china. *Neurotoxicology*, 82:100-107. https://doi.org/10.1016/j.neuro.2020.11.009

Wang YZ, Wang YC, Liu W, et al., 2023. Tim-4 orchestrates mitochondrial homeostasis to promote lung cancer progression via anxa2/pi3k/akt/opa1 axis. *Cell Death Dis*, 14(2):141. https://doi.org/10.1038/s41419-023-05678-3

Xing SP, Zhang CR, Guo HM, et al., 2024. Hydrologic changes induced by groundwater abstraction lead to arsenic mobilization in shallow aquifers. *J Hazard Mater*, 480:136133. https://doi.org/10.1016/j.jhazmat.2024.136133

Yan T, Zhang ZH, Li DQ, 2020. Ngf receptors and pi3k/akt pathway involved in glucose fluctuation-induced damage to neurons and alpha-lipoic acid treatment. *BMC Neurosci*, 21(1):38. https://doi.org/10.1186/s12868-020-00588-y

Yapa NMB, Lisnyak V, Reljic B, et al., 2021. Mitochondrial dynamics in health and disease. *FEBS Lett*, 595(8):1184-1204. https://doi.org/10.1002/1873-3468.14077

Ye FP, Wu L, Li H, et al., 2023. Sirt1/pgc-1alpha is involved in arsenic-induced male reproductive damage through mitochondrial dysfunction, which is blocked by the antioxidative effect of zinc. *Environ Pollut*, 320:121084. https://doi.org/10.1016/j.envpol.2023.121084

Supplementary information

Table S1-S2; Figs. S1-S2